High-Concentration, Surfactant-Stabilized Graphene Dispersions

Mustafa Lotya,[†,‡] Paul J King,[†,‡] Umar Khan,[†,‡] Sukanta De,[†,‡] and Jonathan N Coleman[†,‡,*]

[†]School of Physics, [‡]Centre for Research on Adaptive Nanostructures and Nanodevices (CRANN), Trinity College Dublin, Dublin 2, Ireland

ABSTRACT A method is presented to produce graphene dispersions, stabilized in water by the surfactant sodium cholate, at concentrations up to 0.3 mg/mL. The process uses low power sonication for long times (up to 400 h) followed by centrifugation to yield stable dispersions. The dispersed concentration increases with sonication time while the best quality dispersions are obtained for centrifugation rates between 500 and 2000 rpm. Detailed TEM analysis shows the flakes to consist of 1−10 stacked monolayers with up to 20% of flakes containing just one layer. The average flake consists of ~4 stacked monolayers and has length and width of ~1 μm and ~400 nm, respectively. These dimensions are surprisingly stable under prolonged sonication. However, the mean flake length falls from ~1 μm to ~500 nm as the centrifugation rate is increased from 500 to 5000 rpm. Raman spectroscopy shows the flake bodies to be relatively defect-free for centrifugation rates below 2000 rpm. The dispersions can be easily cast into high-quality, free-standing films. The method extends the scope for scalable liquid-phase processing of graphene for a wide range of applications.

KEYWORDS: graphene · surfactant · sonication

Due to its unique physical properties, graphene has generated intense interest in recent years.[1,2] While much interesting work has been carried out on micromechanically cleaved graphene, for many applications it will be necessary to develop high-yield, high-throughput processing methods.[3] Pioneering work in this area has been carried out by Ruoff and co-workers, who have demonstrated large-scale exfoliation of graphene oxide (GO).[4−6] This material is prepared by acid-treating graphite and consists of graphene sheets decorated with epoxides, carboxyl, and hydroxyl groups. GO is highly exfoliated and very stable when dispersed in aqueous environments. Such dispersions are very useful as they facilitate both materials processing and fundamental characterization. For example, they have been used to deposit individual sheets for spectroscopic analysis,[7,8] prepare polymer−graphene composites,[4] and develop graphene thin films.[9,10]

However, GO is not ideal and suffers from some important drawbacks. Because of the presence of oxides, GO is a poor electrical conductor.[5] While the oxides can be removed by reduction,[5,11,12] this adds yet another step in the processing procedure. A bigger problem is that reduction cannot remove the many structural defects introduced by the oxidation process.[5,13−17] These defects disrupt the band structure and completely degrade the electronic properties that make graphene unique.

In order to address these issues, our group and others have developed techniques to disperse and exfoliate pristine graphene in solvents[18−23] or using surfactants[24−27] without oxidation or defect formation. Surfactant exfoliation is of particular importance as it can be achieved in aqueous environments. Originally, we were only able to disperse graphene at low concentrations, typically <0.01 mg/mL for both solvents and surfactants. Such a low concentration makes many applications completely impractical. This gives graphene oxide a significant advantage as it can be dispersed in some organic solvents at concentrations of up to 1 mg/mL[5,28−30] and in water at concentrations of up to 7 mg/mL.[31] However, we recently showed that graphene could be exfoliated in the solvent *N*-methylpyrrolidone at concentrations of ~1 mg/mL.[22] Extension of this breakthrough to surfactant-exfoliated graphene would be a significant achievement.

In order to gain full advantage from dispersions of pristine graphene using surfactants, it will be critical to increase the maximum concentration obtainable while maintaining the quality of the graphene flakes. In this work, we demonstrate such a method. We show that by applying mild sonication for long times (up to 430 h) graphene can be effectively dispersed in

*Address correspondence
colemaj@tcd.ie

Received for review March 15, 2010
and accepted April 28, 2010.

Published online May 10, 2010.
10.1021/nn1005304

water−sodium cholate solutions at concentrations of up to ~0.3 mg/mL. We use TEM analysis to show that the dispersions consist of extremely well exfoliated flakes. Finally, we show that these dispersions can be used to prepare free-standing films with reasonable electrical and mechanical properties.

RESULTS AND DISCUSSION

Surfactant Exfoliation of Graphene. The goal of this work is to prepare surfactant-stabilized dispersions of graphene at high concentration. In addition, the flakes should be well exfoliated (i.e., few layers per flake), reasonably large, and relatively defect free. Our chosen method for preparing this type of nanomaterial dispersion requires the use of sonication followed by centrifugation. Thus, we expect that optimization of dispersion parameters will result in enhanced final concentration and dispersion quality. The main parameters are initial graphite concentration ($C_{G,i}$), surfactant concentration (C_{NaC}), centrifugation rate (ω), and sonication time (t_{sonic}). We measured the concentration after centrifugation, C_G, by measuring the absorbance spectrum. From the spectra, we measured the absorbance per unit cell length, A/l. From the Lambert−Beer law, this gives the concentration once the extinction coefficient, α_G, is known ($A = \alpha_G C_G l$). We determined the extinction coefficient by measuring A/l at 660 nm for large known volumes of dispersion across a range of ω ($C_{G,i}$ = 5 mg/mL, C_{NaC} = 0.1 mg/mL, t_{sonic} = 24 h, ω from 500 to 5000 rpm). These dispersions (in excess of 400 mL volumes) were filtered through a pre-weighed porous membrane. The membranes were dried and reweighed to give the deposited mass. The proportion of graphitic mass on the filter membrane was determined using TGA analysis. This gave a mean value of α_G = 6600 L g^{-1} m^{-1}. This is significantly higher than our initial measurement of 1390 L g^{-1} m^{-1} in low concentration systems.[25] A plot of the measured data points is given in the Supporting Information, Figure S1.

As we aim to maximize the final dispersed graphene concentration, we chose a reasonably high starting graphite concentration, $C_{G,i}$ = 5 mg/mL. We optimized the surfactant concentration by measuring the concentration of graphene remaining dispersed after sonication and centrifugation as a function of C_{NaC} (t_{sonic} = 24 h, centrifugation: ω = 1000 rpm, t_{CF} = 30 min). We chose the CF rate and time based on our experience with solvent−graphene dispersions.[22] We note that this sonication time is much longer than that used previously for surfactant/graphene systems.[25] The results are shown in Figure 1A (inset). We see that the surfactant concentration peaks strongly at C_{NaC} = 0.1 mg/mL. This is rather surprising: we expected the peak to occur close to the critical micelle concentration of NaC (~5 mg/mL) as was observed for graphene/SDBS dispersions.[25] The reason for the discrepancy is unclear. Nevertheless, we chose to prepare all subsequent dispersions with C_{NaC} = 0.1 mg/mL.

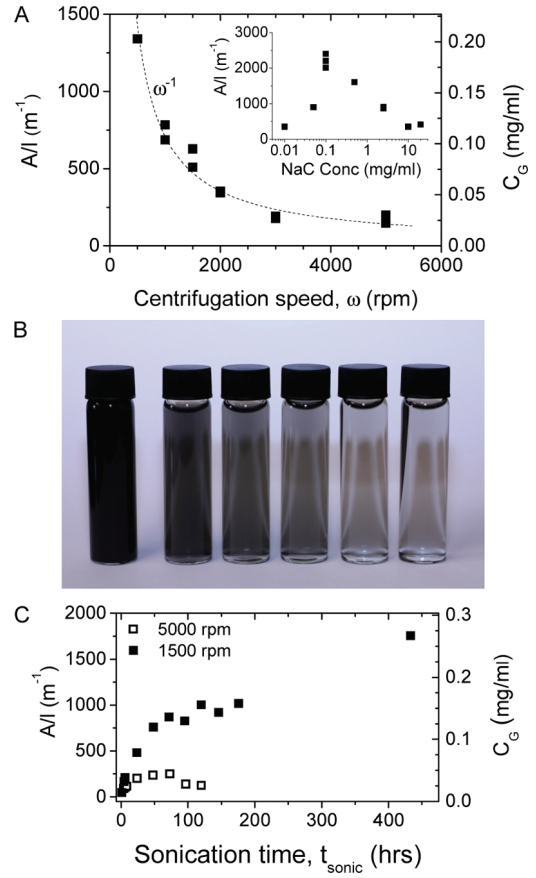

Figure 1. (A) A/l as a function of centrifugation speed ($C_{G,i}$ = 5 mg/mL, C_{NaC} = 0.1 mg/mL, t_{sonic} = 24 h, centrifugation: 90 min). Inset: Absorbance/cell length, A/l, as a function of surfactant concentration (C_G = 5 mg/mL, t_{sonic} = 24 h, centrifugation: 1000 rpm for 30 min). Subsequently, a surfactant concentration of 0.1 mg/mL was used for all dispersions. (B) Photos of surfactant-stabilized graphene dispersions; $C_{G,i}$ = 5 mg/mL, C_{NaC} = 0.1 mg/mL, t_{sonic} = 24 h. Left to right: uncentrifuged, centrifuged for 90 min at 1000 rpm, 1500 rpm, 2000 rpm, 3000 rpm, 5000 rpm. Note that the centrifuged dispersions have been diluted by a factor of 10 to highlight the color change. (C) A/l as a function of sonication time ($C_{G,i}$ = 5 mg/mL, C_{NaC} = 0.1 mg/mL, centrifugation: 90 min) for centrifugation speeds of 5000 and 1500 rpm. Note that in both A and C the right axis shows the graphitic concentration calculated using an absorption coefficient of 6600 L g^{-1} m^{-1}.

The next question was the effect of CF rate on the dispersion. We prepared a stock graphene dispersion ($C_{G,i}$ = 5 mg/mL, C_{NaC} = 0.1 mg/mL, t_{sonic} = 24 h) and centrifuged portions of it at different rates, ω, from 500 to 5000 rpm (25−2500g). In this and all subsequent experiments, the samples were centrifuged for 90 min as we found this to be more effective than 30 min. In all cases, the dispersions were very dark, even after CF. However, on dilution, it was clear to the eye that those samples centrifuged at higher rates had lower concentrations (Figure 1B). In each case, we measured the concentration after centrifugation as shown in Figure 1A. As ω was increased, the concentration decreased from 0.2 mg/mL to 0.03 mg/mL. Interestingly, we observed

an empirical scaling of $C_G \propto \omega^{-1}$, different from the expected ω^{-2} scaling. We note that at this point it is impossible to identify an optimum value of ω as we have no information to differentiate the qualities of the dispersions. We will discuss this later.

The final processing parameter we must explore is the sonication time. Previous work on graphene dispersed in the solvent *N*-methylpyrrolidone (NMP) has shown that the concentration of exfoliated graphene can be increased significantly by increasing the sonication time.[22] Thus, we prepared a large volume of stock dispersion (400 mL dispersion in a 500 mL round bottomed flask, $C_{G,i} = 5$ mg/mL, $C_{NaC} = 0.1$ mg/mL). We bath sonicated this stock for ~430 h. At a number of times during this period, we removed two aliquots of ~5 mL each. These were each centrifuged for 90 min at different rates: 1500 and 5000 rpm. In all cases, the concentration after CF was measured optically. These concentrations are plotted as a function of sonication time, *t*, in Figure 1C. In both cases, the concentration increases dramatically with concentration, reaching values of 0.3 and 0.05 mg/mL for the 1500 and 5000 rpm dispersions, respectively. We note that graphene dispersions prepared in NMP exhibit well-defined behavior characterized by $C_G \propto \sqrt{t_{sonic}}$.[22] While C_G scales sublinearly with t_{sonic}, the data presented in Figure 1C do not scale well with $\sqrt{t_{sonic}}$.

We have shown that the sodium cholate stabilized graphene dispersions can be prepared at reasonably high concentrations, reaching 0.3 mg/mL. This is significantly higher than the maximum values of ~0.06 mg/mL achieved previously.[25] In addition, it is higher than the concentrations of ~0.09 mg/mL obtained by Green *et al.* by intense tip sonication of graphite in sodium cholate.[24] It is not clear why extended low power sonication gives greater concentrations than high power tip sonication. However, it is likely that the cited tip sonication method is not fully optomized and could be tuned to give better results.

In addition, we probed the stability of our dispersions by conducting sedimentation measurements on a typical dispersion ($C_{G,i} = 5$ mg/mL, $C_{NaC} = 0.1$ mg/mL, $t_{sonic} = 24$ h, $\omega = 1500$ rpm, diluted by a factor of 2 in 0.1 mg/mL NaC solution). These data are presented in the Supporting Information, Figure S2, showing that 97% of the sample remained suspended after 5 days. This indicates that the centrifugation regime used yielded very stable dispersions and successfully removed the vast majority of thick objects. This compares very favorably with our earlier work on low concentration graphene/surfactant systems where ~60% of the dispersed material was retained over a similar time frame.[25]

Exfoliation Quality. Despite high yield and good stability, it is critical to evaluate the quality of the dispersions. We do this in two ways; we measure the flake size and thickness by TEM and then assess the defect content by Raman spectroscopy. We choose to measure the flake size by TEM as this method has a number of advantages; sample preparation is straightforward, and the lateral flake dimensions are easily measured. In addition, one can count the numbers of graphene layers per flake by examining the edges of the flakes.[22] In TEM images of graphene multilayers, the edges of the individual flakes are almost always distinguishable. Thus, by carefully counting the flake edges it is possible to measure the number of layers per flake. The downside of this technique is that smaller flakes may be lost through the holes in the grid. This means that data on lateral flake dimensions may be biased toward higher values. We note that most researchers use atomic force microscopy to measure flake thickness and size. We have not done this here. In previous work, we found that the presence of surfactant on the substrate makes AFM characterization difficult. In addition, we were unable to remove all residual surfactant.

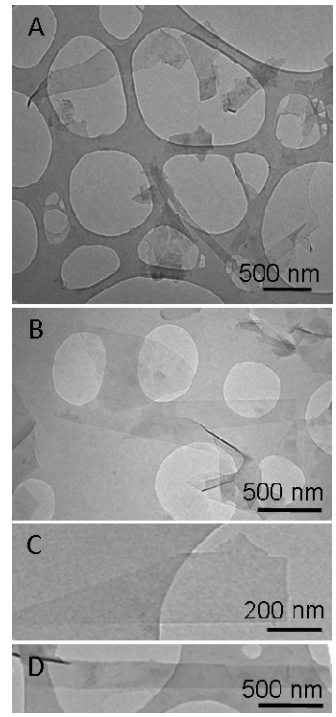

Figure 2. (A) Wide field and (B) closeup TEM images of a highly exfoliated graphene monolayer and multilayer flakes, (C) a monolayer graphene flake, and (D) a graphene ribbon. These samples were deposited from dispersions prepared with the following parameters: (A) $C_{G,i} = 5$ mg/mL, $C_{NaC} = 0.1$ mg/mL, $t_{sonic} = 72$ h, centrifugation: 1500 rpm, 90 min); (B) $C_{G,i} = 5$ mg/mL, $C_{NaC} = 2.5$ mg/mL, $t_{sonic} = 48$ h, centrifugation: 1000 rpm, 30 min); (C and D) $C_{G,i} = 5$ mg/mL, $C_{NaC} = 0.1$ mg/mL, $t_{sonic} = 144$ h, centrifugation: 1500 rpm, 90 min).

We have used TEM to characterize a range of dispersions prepared with sonication times from 6 to 433 h ($\omega = 1500$ rpm) and with rotation rates from 500 to 5000 rpm ($t_{sonic} = 24$ h). Shown in Figure 2A−D are four sample TEM images of exfoliated graphene flakes. In general, we observe well-exfoliated graphene multilayers (Figure 2B) and monolayers (Figure 2C,D). The level of exfoliation can be seen visually by the transparency of the flakes to the e-beam. A few thick objects opaque to the TEM beam were observed across the entire TEM

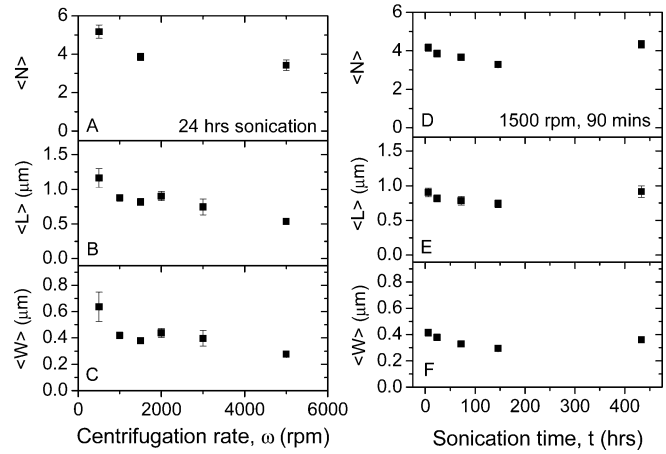

Figure 3. Flake size as a function of sonication time and centrifugation speed: (A) mean number of layers per flake ⟨*N*⟩; (B) mean flake length ⟨*L*⟩; (C) mean flake width ⟨*w*⟩ as a function of centrifugation speed; (D) ⟨*N*⟩, (E) ⟨*L*⟩, and (F) ⟨*w*⟩ as a function of sonication time.

grid at the lowest rotation rate of 500 rpm. We believe these are nanographite particles with approximately 4−15 μm lateral sizes. By examining several low magnification images of samples at 500 rpm ($C_{G,i}$ = 5 mg/mL, C_{NaC} = 0.1 mg/mL, t_{sonic} = 24 h), we estimate the number fraction of these thick objects to be less than 2%. At rotation rates of 1500 rpm and above we observed no such very thick objects in the samples. It is interesting to note that some of the monolayers have relatively large aspect ratios. An example is the ribbon shown in Figure 2D.

We can use TEM images of the type shown in Figure 2 to generate statistical data on the exfoliation state of the graphene in these dispersions. For each flake observed, we measure the length, *L*, and width, *w*, and estimate the number of layers per flake, *N*. To determine *N*, we examine the edges of the individual flakes as described in detail elsewhere.[20,22] For some multilayers, we acknowledge that exact edge counting is not trivial; in such cases, only an estimation of *N* is possible. We expect that the random errors involved will cancel each other out when compiling statistical data. We analyze approximately 100 flakes for each sonication time. We found a monolayer number fraction, N_1/N_T, of ∼10% for the samples prepared at a rotation rate of 1500 rpm for all sonication times. This corresponds to a monolayer mass fraction of ∼1.1 wt %.[20] This is in line with our previous work on liquid-phase graphene exfoliation in solvent systems, suggesting that these yields are controlled by the sonication procedure rather than by the dispersant/stabilizer.[20] We found that the fraction of flakes with <3 layers, N_{1-2}/N_T = 50% while N_{1-4}/N_T = 80%. For the 5000 rpm sample, the population of monolayers was higher at N_1/N_T = 19%. The mean flake aspect ratio ⟨*L*/*w*⟩ was fairly constant between 2.0 and 2.7; this is in agreement with previous work and suggests that sonication-induced exfoliation favors asymmetric flakes.[22] The full results of the flake thickness, length, width, and aspect ratio (*L*/*w*) results are shown in the Supporting Information, Figures S3(A−D) and S4(A−D), as functions of sonication time and rotation rate, respectively.

We can analyze this statistical data in a number of ways. We have calculated the mean number of layers per flake, ⟨*N*⟩, and the mean flake length, ⟨*L*⟩, and width, ⟨*w*⟩, as a function of both CF rate and sonication time. These data are shown in Figure 3A−C and D−E, respectively. As the CF rate is increased, ⟨*N*⟩, ⟨*L*⟩, and ⟨*w*⟩ all decrease to some degree. Going from 500−5000 rpm, ⟨*N*⟩ falls from 5 to 3.5, ⟨*L*⟩ falls from 1.2 to 0.5 μm while ⟨*w*⟩ falls from 600 to 300 nm. It is not surprising that centrifugation preferentially removes the larger flakes, thus reducing the mean flake size. These data are in agreement with our previous work on NMP-dispersed graphene, where we found the flake length and width to fall by a factor of 2 over a similar range of rpm. Surprisingly, as the sonication time is increased, ⟨*N*⟩, ⟨*L*⟩, and ⟨*w*⟩ hardly vary at all, displaying relatively constant values of ∼4, 800, and 350 nm, respectively. For NMP-dispersed graphene, we observed ⟨*L*⟩ and ⟨*w*⟩ to fall as $t^{-1/2}$.[22] Such size reduction was expected and is caused by sonication-induced cutting.[32] The absence of such behavior in the surfactant-dispersed samples suggests that sonication has cut the flakes to a certain size within the first 6 h, but beyond this time, sonication induced scission is suppressed. Sonication-induced scission is a tensile process that relies on stress being transferred from fluid to dispersed object.[32,33] If the transferred stress exceeds the tensile strength of the dispersed object, it will fracture. That fracture becomes rarer for sonication times above 6 h may indicate that the fluid−graphene stress transfer is limited. This can probably be explained by surfactant slippage at the graphene/surfactant/water double interface.

We note that TEM-based stats may be biased by very small flakes being lost through the TEM grid. However, in addition to observing large flakes (length up to few μm), we have observed flakes as small as 50 nm in all

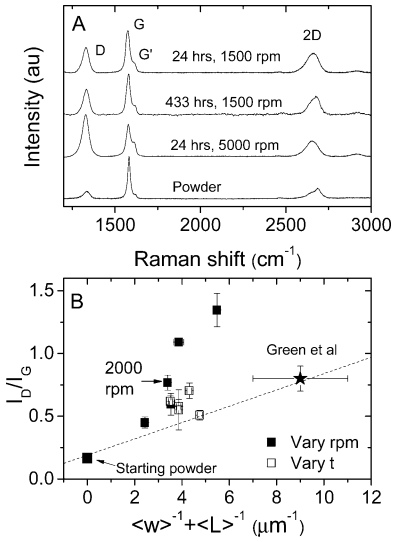

Figure 4. (A) Raman spectra for the starting graphite powder and for thin films prepared from 1500 rpm, 24 h sonication; 1500 rpm, 433 h sonication; and 5000 rpm, 24 h sonication. We note that the D band intensity is surprisingly insensitive to sonication time but increases strongly with increasing centrifugation rate. (B) Ratio of D to G band intensity as a function of mean flake perimeter/mean flake area ($\langle w\rangle^{-1} + \langle L\rangle^{-1}$) for the samples with varying centrifugation speed and varying sonication time. A straight line on this graph would be consistent with edge defects only contributing to the Raman signal. The dashed line represents data previously found for solvent exfoliated graphene, while the star represents the data reported by Green *et al.* for sodium cholate exfoliated graphene. The bottom left most point represents the powder.

cases. We can compare this with results by Green *et al.*, who used a high power sonic tip and observed severe cutting. They used density gradient centrifugation to separate flakes by size. They observed typical flake (lateral) sizes of ~100 nm with maximum sizes of ~250 nm.[24]

Defect Content. We must also consider the defect content of the exfoliated graphene. For all dispersions studied by TEM, we formed thin films by vacuum filtration. For each film, we measured Raman spectra at a number of points on the film. Shown in Figure 4A are representative Raman spectra for the samples with varying sonication time and CF rate [(t_{sonic}/hs, rate/rpm) = (24, 1500), (433, 1500), (24, 5000)]. The spectrum for the starting powder is shown for comparison. The defect content is indicated by the intensity of the D band (~1350 cm^{-1}) relative to the G band (~1580 cm^{-1}). We note that all spectra have D bands significantly larger than that of the starting powder, indicating that processing induces defects. We can divide such defects into two main types: body defects such as point defects on the basal plane and edge defects. The introduction of edge defects is unavoidable during processing as sonication cuts the initially large crystallites up into smaller flakes. These smaller flakes have more edges per unit mass resulting in an increase in edge defect population. We present the mean D/G band intensity ratio, I_D/I_G, for all samples in the Supporting Information, Figure S5. As a function of sonication time (ω = 1500 rpm), the D/G band ratio is surprisingly invariant around an overall mean value of 0.57. This shows that significant quantities of new edges are not being created by prolonged sonication and hence that the flakes are not getting cut dramatically. This is in good agreement with the TEM flake-size data (Figure 3). However, I_D/I_G increases significantly with CF rate, indicating that the flakes retained at higher rotation rates have more defects. This suggests that the flakes retained at higher rotation rates have more basal plane defects and/or are smaller than those obtained at low CF rates.

We can attempt to determine whether the increase in total defect population is due to the introduction of edge or body defects. We do this by noting that, for edges only, the ratio of D to G band intensity must be proportional to the ratio of mean flake edge length to area (because $I_D \propto$ edge length while $I_G \propto$ flake area). Modelling the flakes as rectangles,[22] this means

$$\frac{I_D}{I_G} \propto \frac{1}{\langle L\rangle} + \frac{1}{\langle w\rangle}$$

We can calculate I_D/I_G from the Raman data and ($\langle L\rangle^{-1} + \langle w\rangle^{-1}$) from the TEM statistics. If these quantities scale linearly, with an I_D/I_G intercept close to the value of I_D/I_G for the powder, we can conclude the introduced defects are due to new edges only. We have calculated these quantities for both data sets (varying t_{sonic} and ω) and plotted them in Figure 4B. It is clear from this graph that these data do not sit on one straight line. This is in contrast to results we obtained for NMP-dispersed graphene where all data (like here from samples with varying t and ω) sat on a well-defined straight line.[22] We will consider the sonication time data first. Here, I_D/I_G does not vary much because the flake size did not vary significantly with sonication time. Thus, the open squares in Figure 4B are clustered. However, we note that for NMP dispersions[22] we found that the data scaled as $I_D/I_G = 0.19 + 0.065(\langle L\rangle^{-1} + \langle w\rangle^{-1})$. This curve is plotted in Figure 4B as the dashed line. We find that all the sonication time data and the rpm data with $\omega < 2000$ rpm sit reasonably close to this line. In addition, if we take the flake size and Raman data from Green *et al.* and plot it in Figure 4B (filled star), it also sits very close to this line. This means that the majority of our data, as well as Green's data, are consistent with the formation of edge defects during sonication. However, the ω-dependent data tend to deviate from the line for rates >2000 rpm. Part of this discrepancy may be explained by the loss of small flakes through the grid for the higher rpm samples resulting in an overestimation of flake size. However, the true values of $\langle L\rangle$ and $\langle w\rangle$ would have to be exceptionally low (required values of $\langle L\rangle$ = 190 nm, $\langle w\rangle$ = 95 nm at 5000 rpm) for this to fully explain the data. Thus, it appears clear that flakes processed using our procedure and centrifuged at rates greater than 2000 rpm tend

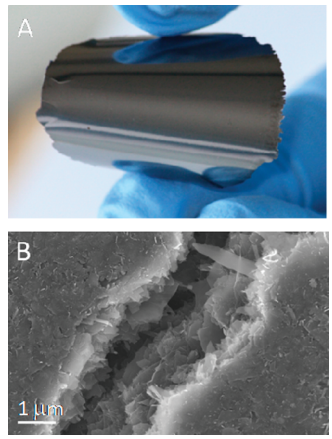

Figure 5. (A) Free-standing film prepared from a NaC/graphene dispersion ($C_{G,i}$ = 5 mg/mL, C_{NaC} = 0.1 mg/mL, t_{sonic} = 171 h, centrifugation: 1000 rpm, 30 min). (B) SEM image of a crack on the surface of a free-standing film ($C_{G,i}$ = 5 mg/mL, C_{NaC} = 0.1 mg/mL, t_{sonic} = 24 h, centrifugation: 1500 rpm, 90 min).

to have excess body defects. It is possible that flakes with body defects are more stable against sedimentation at high rotation rates, although the mechanism for this remains a mystery. In any case, these data suggest that the defect population is dominated by edge defects for rates <2000 rpm. By extension, this suggests that the samples prepared at lower rpm have low levels of body defects. This gives us our criterion to determine the optimized rpm for our system. The rotation rates used should be above 500 rpm (the minimum required to remove large aggregates) but below 2000 rpm (where body defects begin to dominate).

We can also consider the 2D band. The shape of this band is indicative of the number of layers per flake.[34,35] For flakes thinner than ~5 layers, the Raman spectrum is considerably different from that of graphene. None of the spectra measured for the thin films described above displayed graphite-like character. Rather, all spectra were consistent with flakes of three to five layers in good agreement with the TEM data.

Film Formation. Surfactant-stabilized graphene dispersions can be used in a range of applications. We have already shown that they can be used to prepare transparent conducting thin films.[27] In addition, we expect a role for them in the formation of composites of graphene with water-soluble polymers. In fact, by analogy with carbon nanotubes, the ability to prepare good-quality, water-based dispersions should facilitate many applications. Here, we demonstrate that such dispersions can be used to prepare free-standing films. These were prepared by vacuum filtration onto porous alumina membranes followed by drying in a 70 °C oven. Although we prepared free-standing films with thickness in the range 50−120 μm, there is no real limit to what can be done. We have already demonstrated the preparation of films with thickness as low as 10 nm.[27] Thicker films can be easily peeled from the filter membrane. They tend to be shiny on the side which faced the membrane but matt black on the other side. They are surprisingly robust and can be mildly bent and flexed without breaking (see Figure 5A). These films display densities between 1000 and 1440 kg/m^3. This figure includes the effects of residual surfactant. These densities correspond to porosities between ~55 and ~35%. By performing thermogravimetric analysis on the films, we can correct for the residual surfactant content giving graphitic density of between 850 and 1050 kg/m^3. SEM analysis shows the films to consist of graphene flakes well aligned in the plane of the film (Figure 5B). Raman analysis of these films shows 2D bands consistent with graphene flakes of three to five layers. This shows that while the graphene must aggregate to form the film, the flakes do not aggregate in an ordered way (i.e., do not AB stack), but rather small multilayers tend to restack randomly on top of each other. This random stacking retains the electronic structure of the multilayers resulting in the observed Raman spectra.[35] These free-standing films have Young's moduli ranging from ~4 to ~10 GPa (Supporting Information, Figure S6). Ultimate tensile strengths ranged from 15 to 33 MPa. These values are similar to free-standing films we made from NMP/graphene dispersions but lower than reported values for graphene oxide[36,37] and reduced graphene oxide films.[36,38] This is probably due to the presence of residual surfactant in our films, measured at between 15 and 30% by TGA analysis. These films have mean conductivity of 7000 S/m before annealing, comparable to films made from reduced graphene oxide without annealing.[38] The mean conductivity rises to 17500 S/m after annealing at 500 °C for 2 h under argon/hydrogen atmosphere (Supporting Information, Figure S7). Again, this value closely matches that measured for free-standing graphene films from NMP dispersions and compares favorably to reduced graphene oxide films that have been annealed.[36]

CONCLUSIONS

In conclusion, we have demonstrated a low-cost and scalable process to prepare stable dispersions of graphene at concentrations up to 0.3 mg/mL in surfactant/water systems. The dispersed concentration increases sublinearly with sonication time, while high-quality dispersions are obtained for centrifugation rates between 500 and 2000 rpm. The process yields a monolayer number fraction of ~10% (1 wt %) with a large proportion of material consisting of less than five graphene layers (up to 80% of flakes). The scaling of Raman D-band to G-band intensity ratio (I_D/I_G) with sonication time is consistent with new edges being formed. However, the I_D/I_G scaling with centrifuge rotation rate may indicate an excess of body defects in the smaller graphene flakes produced. The dispersions can be easily cast into free-standing films with good electrical and

mechanical properties. We believe this method will support the development of a range of new graphene-based composite materials that require aqueous precursors.

EXPERIMENTAL METHODS

Natural flake graphite was purchased from Branwell Graphite Ltd. (Grade RFL 99.5, cost ~$5 kg^{-1}) and used as provided. Sodium cholate (NaC) was purchased from Sigma Aldrich (SigmaUltra >99%) and was dissolved in Millipore water at various concentrations between 0.01 and 20 mg/mL. Graphene dispersions were prepared by adding graphite at an initial concentration of $C_{G,i}$ = 5 mg/mL to 400 mL NaC solution in 500 mL capped round-bottomed flasks. Various surfactant concentrations (C_{NaC}) were explored. Ultrasonication was carried out in a low power sonic bath (Branson 1510E-MT). While the nominal power output for this bath was 80 W, we estimated the true power output (by measuring the temperature increase while sonicating a known mass of water) to be 16 W. Due to the long sonication times used in these experiments, continuous refilling of bath water by siphoning from a water reservoir was necessary to maintain sonication efficiency and prevent overheating. Samples extracted from the flasks by pipet (10−28 mL) were left to stand overnight to allow any large unstable graphite aggregates to form and then centrifuged in 14−28 mL glass vials for times (t_{CF}) of either 30 or 90 min (Hettich Mickro 22R and Hettich Mickro 220R). After centrifugation (CF), the top two-thirds of th edispersion was extracted by pipet and retained for use.

Optical absorption measurements were taken with a Varian Cary 50 and Cary 6000i using optical grade glass or quartz cuvettes. Sedimentation measurements were performed with a homemade apparatus consisting of an array of synchronized pulsed lasers and photodiodes.[32] Samples for TEM analysis were prepared by drop-casting a few milliliters of dispersion onto holey carbon grids (400 mesh). Bright-field TEM images were taken with a JEOL 2100, operated at 200 kV.

Deposited thin films were prepared by vacuum filtration onto porous mixed cellulose ester membranes (Millipore, 0.025 μm pore size, 47 mm diameter). Free-standing films were prepared by vacuum filtration onto porous alumina membranes (Millipore, 0.02 μm pore size, 47 mm membrane diameter, final graphene film diameter 36 mm) and drying in a 70 °C oven. The Raman measurements were made on these films with a Horiba Jobin Yvon LAbRAM-HR using a 633 nm laser and either 100× or 10× objective lenses. In all cases, five spectra were collected, and the I_D/I_G ratio was averaged. SEM analysis was carried with a Zeiss Ultra Plus SEM. Thermogravimetric (TGA) analysis was performed on a Perkin-Elmer Pyris 1 in an oxygen atmosphere.

Acknowledgment. We acknowledgement financial support from Science Foundation Ireland through the principle investigator program (Grant No. 07/IN.1/I1772). M.L. thanks IRCSET for support.

Supporting Information Available: Figures S1−S7. This material is available free of charge *via* the Internet at http://pubs.acs.org.

REFERENCES AND NOTES

1. Geim, A. K. Graphene: Status and Prospects. *Science* **2009**, *324*, 1530–1534.
2. Geim, A. K.; Novoselov, K. S. The Rise of Graphene. *Nat. Mater.* **2007**, *6*, 183–191.
3. Ruoff, R. Calling All Chemists. *Nat. Nanotechnol.* **2008**, *3*, 10–11.
4. Stankovich, S.; Dikin, D. A.; Dommett, G. H. B.; Kohlhaas, K. M.; Zimney, E. J.; Stach, E. A.; Piner, R. D.; Nguyen, S. T.; Ruoff, R. S. Graphene-Based Composite Materials. *Nature* **2006**, *442*, 282–286.
5. Stankovich, S.; Dikin, D. A.; Piner, R. D.; Kohlhaas, K. A.; Kleinhammes, A.; Jia, Y.; Wu, Y.; Nguyen, S. T.; Ruoff, R. S. Synthesis of Graphene-Based Nanosheets Via Chemical Reduction of Exfoliated Graphite Oxide. *Carbon* **2007**, *45*, 1558–1565.
6. Stankovich, S.; Piner, R. D.; Chen, X. Q.; Wu, N. Q.; Nguyen, S. T.; Ruoff, R. S. Stable Aqueous Dispersions of Graphitic Nanoplatelets Via the Reduction of Exfoliated Graphite Oxide in the Presence of Poly(Sodium 4-Styrenesulfonate). *J. Mater. Chem.* **2006**, *16*, 155–158.
7. Jung, I.; Pelton, M.; Piner, R.; Dikin, D. A.; Stankovich, S.; Watcharotone, S.; Hausner, M.; Ruoff, R. S. Simple Approach for High-Contrast Optical Imaging and Characterization of Graphene-Based Sheets. *Nano Lett.* **2007**, *7*, 3569–3575.
8. Jung, I.; Vaupel, M.; Pelton, M.; Piner, R.; Dikin, D. A.; Stankovich, S.; An, J.; Ruoff, R. S. Characterization of Thermally Reduced Graphene Oxide by Imaging Ellipsometry. *J. Phys. Chem. C* **2008**, *112*, 8499–8506.
9. Wang, X.; Zhi, L. J.; Mullen, K. Transparent, Conductive Graphene Electrodes for Dye-Sensitized Solar Cells. *Nano Lett.* **2008**, *8*, 323–327.
10. Wu, J. B.; Becerril, H. A.; Bao, Z. N.; Liu, Z. F.; Chen, Y. S.; Peumans, P. Organic Solar Cells with Solution-Processed Graphene Transparent Electrodes. *Appl. Phys. Lett.* **2008**, *92*, 263302.
11. Jung, I.; Dikin, D. A.; Piner, R. D.; Ruoff, R. S. Tunable Electrical Conductivity of Individual Graphene Oxide Sheets Reduced At "Low" Temperatures. *Nano Lett.* **2008**, *8*, 4283–4287.
12. Park, S.; An, J. H.; Jung, I. W.; Piner, R. D.; An, S. J.; Li, X. S.; Velamakanni, A.; Ruoff, R. S. Colloidal Suspensions of Highly Reduced Graphene Oxide in a Wide Variety of Organic Solvents. *Nano Lett.* **2009**, *9*, 1593–1597.
13. Eda, G.; Fanchini, G.; Chhowalla, M. Large-Area Ultrathin Films of Reduced Graphene Oxide as a Transparent and Flexible Electronic Material. *Nat. Nanotechnol.* **2008**, *3*, 270–274.
14. Gomez-Navarro, C.; Weitz, R. T.; Bittner, A. M.; Scolari, M.; Mews, A.; Burghard, M.; Kern, K. Electronic Transport Properties of Individual Chemically Reduced Graphene Oxide Sheets. *Nano Lett.* **2007**, *7*, 3499–3503.
15. Kang, H.; Kulkarni, A.; Stankovich, S.; Ruoff, R. S.; Baik, S. Restoring Electrical Conductivity of Dielectrophoretically Assembled Graphite Oxide Sheets by Thermal and Chemical Reduction Techniques. *Carbon* **2009**, *47*, 1520–1525.
16. Kudin, K. N.; Ozbas, B.; Schniepp, H. C.; Prud'homme, R. K.; Aksay, I. A.; Car, R. Raman Spectra of Graphite Oxide and Functionalized Graphene Sheets. *Nano Lett.* **2008**, *8*, 36–41.
17. Yang, D.; Velamakanni, A.; Bozoklu, G.; Park, S.; Stoller, M.; Piner, R. D.; Stankovich, S.; Jung, I.; Field, D. A.; Ventrice, C. A.; Ruoff, R. S. Chemical Analysis of Graphene Oxide Films after Heat and Chemical Treatments by X-Ray Photoelectron and Micro-Raman Spectroscopy. *Carbon* **2009**, *47*, 145–152.
18. Blake, P.; Brimicombe, P. D.; Nair, R. R.; Booth, T. J.; Jiang, D.; Schedin, F.; Ponomarenko, L. A.; Morozov, S. V.; Gleeson, H. F.; Hill, E. W.; Geim, A. K.; Novoselov, K. S. Graphene-Based Liquid Crystal Device. *Nano Lett.* **2008**, *8*, 1704–1708.
19. Bourlinos, A. B.; Georgakilas, V.; Zboril, R.; Steriotis, T. A.; Stubos, A. K. Liquid-Phase Exfoliation of Graphite Towards Solubilized Graphenes. *Small* **2009**, *5*, 1841–1845.
20. Hernandez, Y.; Nicolosi, V.; Lotya, M.; Blighe, F. M.; Sun, Z. Y.; De, S.; McGovern, I. T.; Holland, B.; Byrne, M.; Gun'ko, Y. K.; Boland, J. J.; Niraj, P.; Duesberg, G.; Krishnamurthy, S.; Goodhue, R.; Hutchison, J.; Scardaci, V.; Ferrari, A. C.;

Coleman, J. N. High-Yield Production of Graphene by Liquid-Phase Exfoliation of Graphite. *Nat. Nanotechnol.* **2008**, *3*, 563–568.
21. Hamilton, C. E.; Lomeda, J. R.; Sun, Z. Z.; Tour, J. M.; Barron, A. R. High-Yield Organic Dispersions of Unfunctionalized Graphene. *Nano Lett.* **2009**, *9*, 3460–3462.
22. Khan, U.; O'Neill, A.; Lotya, M.; De, S.; Coleman, J. N. High-Concentration Solvent Exfoliation of Graphene. *Small* **2010**, *6*, 864–871.
23. Hernandez, Y.; Lotya, M.; Rickard, D.; Bergin, S. D.; Coleman, J. N. Measurement of Multicomponent Solubility Parameters for Graphene Facilitates Solvent Discovery. *Langmuir* **2010**, *26*, 3208–3213.
24. Green, A. A.; Hersam, M. C. Solution Phase Production of Graphene with Controlled Thickness Via Density Differentiation. *Nano Lett.* **2009**, *9*, 4031–4036.
25. Lotya, M.; Hernandez, Y.; King, P. J.; Smith, R. J.; Nicolosi, V.; Karlsson, L. S.; Blighe, F. M.; De, S.; Wang, Z. M.; McGovern, I. T.; Duesberg, G. S.; Coleman, J. N. Liquid Phase Production of Graphene by Exfoliation of Graphite in Surfactant/Water Solutions. *J. Am. Chem. Soc.* **2009**, *131*, 3611–3620.
26. Vadukumpully, S.; Paul, J.; Valiyaveettil, S. Cationic Surfactant Mediated Exfoliation of Graphite into Graphene Flakes. *Carbon* **2009**, *47*, 3288–3294.
27. De, S.; King, P. J.; Lotya, M.; O'Neill, A.; Doherty, E. M.; Hernandez, Y.; Duesberg, G. S.; Coleman, J. N. Flexible, Transparent, Conducting Films of Randomly Stacked Graphene from Surfactant-Stabilized, Oxide-Free Graphene Dispersions. *Small* **2009**, *6*, 458–464.
28. Lomeda, J. R.; Doyle, C. D.; Kosynkin, D. V.; Hwang, W. F.; Tour, J. M. Diazonium Functionalization of Surfactant-Wrapped Chemically Converted Graphene Sheets. *J. Am. Chem. Soc.* **2008**, *130*, 16201–16206.
29. Tung, V. C.; Allen, M. J.; Yang, Y.; Kaner, R. B. High-Throughput Solution Processing of Large-Scale Graphene. *Nat. Nanotechnol.* **2009**, *4*, 25–29.
30. Williams, G.; Seger, B.; Kamat, P. V. Tio2-Graphene Nanocomposites. Uv-Assisted Photocatalytic Reduction of Graphene Oxide. *ACS Nano* **2008**, *2*, 1487–1491.
31. Park, S.; An, J. H.; Piner, R. D.; Jung, I.; Yang, D. X.; Velamakanni, A.; Nguyen, S. T.; Ruoff, R. S. Aqueous Suspension and Characterization of Chemically Modified Graphene Sheets. *Chem. Mater.* **2008**, *20*, 6592–6594.
32. Hennrich, F.; Krupke, R.; Arnold, K.; Rojas Stutz, J. A.; Lebedkin, S.; Koch, T.; Schimmel, T.; Kappes, M. M. The Mechanism of Cavitation-Induced Scission of Single-Walled Carbon Nanotubes. *J. Phys. Chem. B* **2007**, *111*, 1932–1937.
33. Lucas, A.; Zakri, C.; Maugey, M.; Pasquali, M.; van der Schoot, P.; Poulin, P. Kinetics of Nanotube and Microfiber Scission under Sonication. *J. Phys. Chem. C* **2009**, *113*, 20599–20605.
34. Ferrari, A. C.; Meyer, J. C.; Scardaci, V.; Casiraghi, C.; Lazzeri, M.; Mauri, F.; Piscanec, S.; Jiang, D.; Novoselov, K. S.; Roth, S.; Geim, A. K. Raman Spectrum of Graphene and Graphene Layers. *Phys. Rev. Lett.* **2006**, 97.
35. Malard, L. M.; Pimenta, M. A.; Dresselhaus, G.; Dresselhaus, M. S. Raman Spectroscopy in Graphene. *Phys. Rep. Rev. Sect. Phys. Lett.* **2009**, *473*, 51–87.
36. Chen, H.; Muller, M. B.; Gilmore, K. J.; Wallace, G. G.; Li, D. Mechanically Strong, Electrically Conductive, and Biocompatible Graphene Paper. *Adv. Mater.* **2008**, *20*, 3557.
37. Dikin, D. A.; Stankovich, S.; Zimney, E. J.; Piner, R. D.; Dommett, G. H. B.; Evmenenko, G.; Nguyen, S. T.; Ruoff, R. S. Preparation and Characterization of Graphene Oxide Paper. *Nature* **2007**, *448*, 457–460.
38. Li, D.; Muller, M. B.; Gilje, S.; Kaner, R. B.; Wallace, G. G. Processable Aqueous Dispersions of Graphene Nanosheets. *Nat. Nanotechnol.* **2008**, *3*, 101–105.